Capillarity

Vol. 5, No. 5, p. 83-90, 2022

Original article

Experimental and numerical analysis of imbibition processes in a corrugated capillary tube

Junjie Wang[1], Amgad Salama[2], Jisheng Kou[1]*

[1]*Key Laboratory of Rock Mechanics and Geohazards of Zhejiang Province, Shaoxing 312000, P. R. China*
[2]*Faculty of Engineering and Applied Science, University of Regina, Regina S4S 0A2, Canada*

Keywords:
Lucas-Washburn equation
imbibition model
Tolman length
capillarity
fluid-wall friction

Cited as:
Wang, J., Salama, A., Kou, J. Experimental and numerical analysis of imbibition processes in a corrugated capillary tube. Capillarity, 2022, 5(5): 83-90.
https://doi.org/10.46690/capi.2022.05.01

Abstract:
Spontaneous imbibition is a capillary-driven flow phenomenon that exists widely in nature and is important for several industries. Recently, Tolman length has been introduced to improve the classical Lucas-Washburn imbibition model, in order to alleviate the deviations in calculating the capillary pressure. However, imbibition experiments to measure Tolman length have been scarce. In addition, the fluid-wall friction has a considerable impact on the imbibition process, while it is often ignored. In this work, imbibition experiments under specific conditions are carried out to measure the values of Tolman length, and the fluid-wall friction is taken into consideration in the equilibrium equation. The water uptake model in fractures is adopted to make corrections to the rise of water level. The experimental results show that Tolman length decreases first and then rises with the increasing curvature radius of liquid-gas interface. The data reveal that the Tolman length-based model can better describe the real imbibition processes than the classical Lucas-Washburn model.

1. Introduction

The spontaneous imbibition process of wetting fluid in the matrix significantly influences the slope stability under rainfall conditions, the oil production rate, and the degree of combination of ink and coating (Aslannejad et al., 2021). For instance, when water flooding is employed to recover oil from reservoirs, a certain amount of injected water is usually imbibed into the tight matrix due to the relatively strong capillary force. As a result, the oil recovery rate can be considerably enhanced.

Due to its significance, spontaneous imbibition has attracted a lot of attention in recent years. The classical Lucas-Washburn (LW) imbibition model was established on the basis of assumptions that the capillary segment is equally circular, the tube axis is straight, the fluid is Newtonian, and the contact angle between fluid and tube wall is constant (Lucas, 1918; Washburn, 1921). Many theoretical analyses and experimental studies on imbibition were based on the LW model (Cai et al., 2022). The pore structure can be mathematically described by analytical geometry, therefore the LW imbibition model can better describe the mathematical relationship between capillary rising height and filling degree with time. Subsequently, a number of researchers have improved the LW imbibition model through relaxing the above assumptions (Cai et al., 2021), so as to describe the real phenomena more accurately, and by considering parameters such as the connectivity of capillary assembly, non-straight capillary axis, and non-circular cross-section (Mayer et al., 1965; Mason et al., 1991; Kim et al., 1997; Markl et al., 2018; Brabazon et al., 2019). The effects of fluid and solid properties as well as the geometric scales on the imbibition have also been investigated (Cai et al., 2010; Cito et al., 2012; Salama, 2021; Wang et al., 2021). Recently, the Tolman length-based modified LW imbibition model has been proposed by Wang et al. (2021) to improve the

*Corresponding author.
E-mail address: JunjieWangmail@163.com (J. Wang); Amgad.Salama@uregina.ca (A. Salama); koujisheng@163.com (J. Kou).

Yandy Scientific Press

2207-9963
Received May 25, 2022; revised July 14, 2022; accepted August 5, 2022; available online August 10, 2022.

accuracy by considering the surface tension of a small liquid drop involving the Tolman length rather than its planar value. Tolman length is defined as the difference between the radius of curvature of the equimolar surface (no molecule exists at the interface with this radius) and the radius of curvature of the Gibbs tension surface (the interface with the minimum tension value at this radius). It describes the relationship between the planar and the curved surface tensions, which satisfies the following equation (Tolman, 1949):

$$\frac{\gamma}{\gamma_\infty} = \frac{1}{1+\frac{2\delta_T}{R}} \tag{1}$$

where γ denotes the surface tension of a surface with radius of curvature R, γ_∞ denotes the surface tension of a planar surface, δ_T denotes the Tolman length, and R is the radius of curvature. However, Tolman length is an empirical parameter that relates to fluid and capillary material properties, interface size, temperature, and other factors (Tolman, 1949; Bhatt et al., 2015; Rekhviashvili, 2020). As a result, it is highly necessary to design and conduct high-quality laboratory experiments that can provide real physical parameters under specific conditions as well as validate and verify the models.

In the experimental study of the LW model, some scholars have studied the imbibition process under different conditions through customized experimental methods. For example, an experimental method for the quantification of spontaneous imbibition in geologic materials has been proposed (Zahasky et al., 2019), which makes it possible to perform spontaneous imbibition experiments under high-pressure conditions associated with environmental and energy resource applications. Computed tomography revealed a new time-independent scale relationship that can describe the local imbibition rate as a function of water saturation (Zahasky et al., 2019). Moreover, the effect of pore structure on counter-current imbibition has been studied and one-dimensional counter-current imbibition experiments have been conducted in packed porous media with different pore structures (Meng et al., 2022). Considering the wettability, mineral compositions and pore structures, researchers have established a schematic diagram to reveal the fluid mobility mechanism (Tian et al., 2022). The effects of water injection rate and initial water saturation on oil recovery by imbibition were also studied (Karimaie et al., 2007). A spontaneous imbibition technique combined with nuclear magnetic resonance has been presented to probe the shale pore connectivity of a set of shales with low-medium maturity from the Shahejie Formation of the Jiyang depression (Wang et al., 2021). An imbibition model taking into account the influencing factors of imbibition in tight oil reservoirs was established on the basis of experiments (Wang et al., 2019). The capillary absorption kinetics of concrete-ethylene glycol system have been studied with respect to concrete matrix porosity and liquid viscosity (Hanžič et al., 2010) to validate the LW model. Schoelkopf et al. (2002) analyzed the applicability of the LW model to real network structures. The experimental results revealed a long timescale macroscopic absorption rate depending on the square root of time, but show a failure to perform scaling according to pore size in the LW equation, even though the constants of surface energy, contact angle and fluid viscosity have been retained. Furthermore, the average measured values of pore radius are shown to be finer than the LW-predicted equivalent hydraulic capillary radii (Schoelkopf et al., 2002).

As stated above, although some progress has been made in the experimental study of the LW imbibition model, imbibition experiments to measure the Tolman length are still scarce. In this paper, imbibition experiments are conducted and Tolman length is determined in the modified LW model. The numerical results fit well with the experimental data. As the fluid-wall friction is ignored in conventional models, to accurately describe the real conditions, we add fluid-wall friction to the resistance term in the equilibrium equation of forces.

The rest of this paper is organized as follows. In Section 2, Tolman length is measured experimentally and is derived from the water injection length and the flow velocity field. In Section 3, Tolman length and fluid-wall friction are taken into consideration in the modified LW imbibition model, and numerical simulation is carried out to calculate the instantaneous injection length and velocity of water under certain conditions. In Section 4, the experimental results and numerical simulation are compared to verify the effect of Tolman length on the LW imbibition model. The conclusions are presented in Section 5.

2. Experimental section

In this experiment, a high-speed camera is used to record the imbibition process of water in a custom-made capillary, and the position data after processing are compared with the numerical simulation results. The values of Tolman length are selected through fitting the numerical results with those of experiments.

As shown in Fig. 1, the experimental system mainly contains a glass tank, glass capillary, glass rod, copper wire, scale, beaker, pure water, high-speed camera, tripod, light source, sulfate paper, computer, and air conditioner.

The experimental steps are described as follows: turn on the air conditioner to 20 °C in advance and inject an appropriate amount of pure water into the glass tank. When the water temperature reaches 20 °C, the glass rod is placed horizontally on the upper edge of the glass tank, and the capillary tube is placed on the glass rod. When it is necessary to lower the capillary height, copper wire is used instead of a glass rod for the adjustment. Sulfate paper is stuck on the outer wall of the glass tank, and a light source is placed at the same height behind the sulfate paper. The computer image acquisition software is loaded, the real-time video images are analyzed, and the height, elevation angle and direction of the high-speed camera are adjusted manually to ensure that the lens center and the bottom of the capillary are in the same horizontal plane. The aperture and focal length are adjusted to ensure the clarity of the observed images. The shooting rate is set to control the time interval between two adjacent images. After shooting is started, a proper amount of pure water is taken from a beaker and slowly poured into the glass tank. Water pouring is stopped when the water covers the entrance at the bottom of the capillary. The shooting continues until the imbibition process is completed. The collected photos are

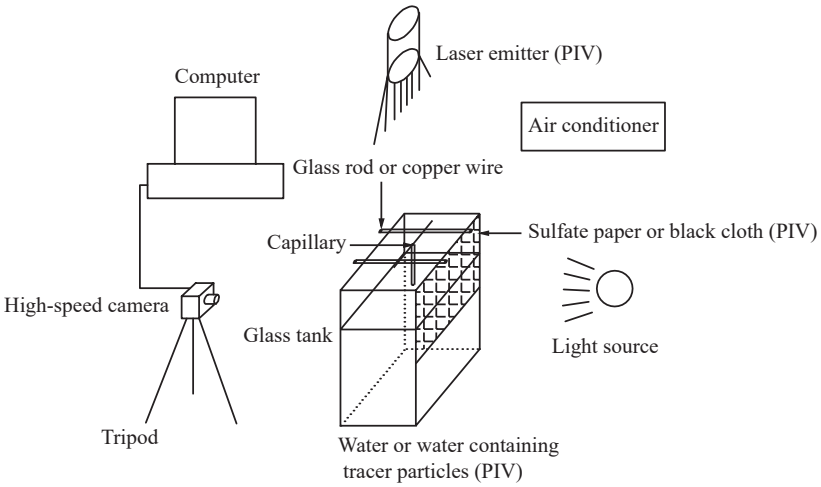

Fig. 1. Experimental equipment.

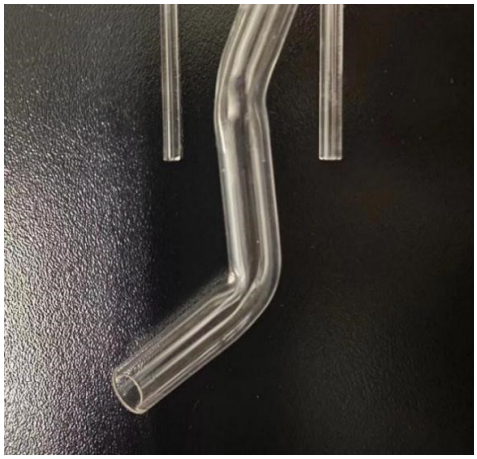

Fig. 2. Three kinds of capillary tubes.

screened, and images between the beginning and the end of imbibition are disregarded. The injection length of water in the photo is measured by a ruler or computer aided design, and the actual injection length of water is calculated by the proportion of the photograph and the real object.

A capillary tube with different specifications is selected for the experiment. The specifications of capillary tubes are shown in Table 1, and their photographs are presented in Fig. 2.

Initial velocity is an important parameter in the numerical calculation, which can make the numerical simulation well predict the capillary imbibition process. The imbibition velocity field of water in a circular tube under certain conditions can be measured by particle image velocimetry (PIV). The experimental system of PIV is shown in Fig. 1, which is similar to the measurement procedure of the imbibition velocity field by PIV. In this setup, it is necessary to add tracer particles into water as well as replace the light source with a laser emitter.

3. Numerical simulation

Our previous work (Wang et al., 2021) proposed a modified LW imbibition model based on Tolman length and an effective numerical method to calculate numerical solutions of the corresponding nonlinear differential equation. Tolman length was taken into account in this model, which can alleviate the deviations between numerical results and real values (Kou et al., 2016). The modified model proposed in this paper considers the effect of fluid-wall friction in the resistance term, which makes the model better describe the real conditions. The shape and size of the capillary tube used in this experiment correspond to the constant radius model and the variable inclination angle model. The model with constant radius is expressed as:

$$\begin{aligned}&\frac{2\gamma\cos\theta}{r}\left[1-\frac{\delta_{\mathrm{T}}\cos\theta}{r}+\mathrm{O}\left(r^{-1}\right)\right]=\rho_{\mathrm{w}}gh\sin\alpha\\&+\frac{\mu h}{K}\frac{\partial h}{\partial t}+\frac{\rho_{\mathrm{w}}\partial\left(h\frac{\partial h}{\partial t}\right)}{\partial t}+\frac{2\rho_{\mathrm{w}}h}{r}\left(\frac{\partial h}{\partial t}\right)^2\end{aligned}\tag{2}$$

where θ denotes the wetting angle, r denotes the tube radius, $\mathrm{O}\left(r^{-1}\right)$ denotes the higher-order infinitesimal of r^{-1}, ρ_{w} denotes the density of the wetting liquid, g denotes the gravitational acceleration, h denotes the total injection length of the wetting liquid, α denotes the inclination angle, K denotes the phase permeability of wetting liquid, μ denotes the dynamic viscosity coefficient of wetting liquid, and t stands for time. The expression of the variable inclination angle model is:

$$\begin{aligned}&\sum_{k=1}^{i-1}\frac{\rho_{\mathrm{w}}g\pi r^2h_k\sin\alpha_k+8\mu h_k\pi\frac{\partial h}{\partial t}+\rho_{\mathrm{w}}\pi h_kr^2\frac{\partial^2h}{\partial t^2}+2\pi r\rho_{\mathrm{w}}h_k\left(\frac{\partial h}{\partial t}\right)^2}{\prod_{j=k+1}^{i}\cos\left(\alpha_j-\alpha_{j-1}\right)}\\&+\rho_{\mathrm{w}}g\pi r^2\left(h-\sum_{j=1}^{i-1}h_j\right)\sin\alpha_i+8\mu\left(h-\sum_{j=1}^{i-1}h_j\right)\pi\frac{\partial h}{\partial t}\\&+\rho_{\mathrm{w}}\pi r^2\left[\left(h-\sum_{j=1}^{i-1}h_j\right)\frac{\partial^2h}{\partial t^2}+\left(\frac{\partial h}{\partial t}\right)^2\right]\\&+2\pi r\rho_{\mathrm{w}}\left(h-\sum_{j=1}^{i-1}h_j\right)\left(\frac{\partial h}{\partial t}\right)^2\\&=2\pi\gamma\cos\theta r\left(1-\frac{\delta_{\mathrm{T}}\cos\theta}{r}+\mathrm{O}\left(r^{-1}\right)\right)\end{aligned}\tag{3}$$

Table 1. Specifications of capillary selected for the experiment.

Serial number	Tube section length (mm)			Inner radius (mm)			Angle of inclination (°)		
1	20 (1st)	20 (2nd)	20 (3rd)	2.5 (1st)	2.5 (2nd)	2.5 (3rd)	44 (1st)	99 (2nd)	44 (3rd)
2	27			0.25			89		
3	21			0.5			90		

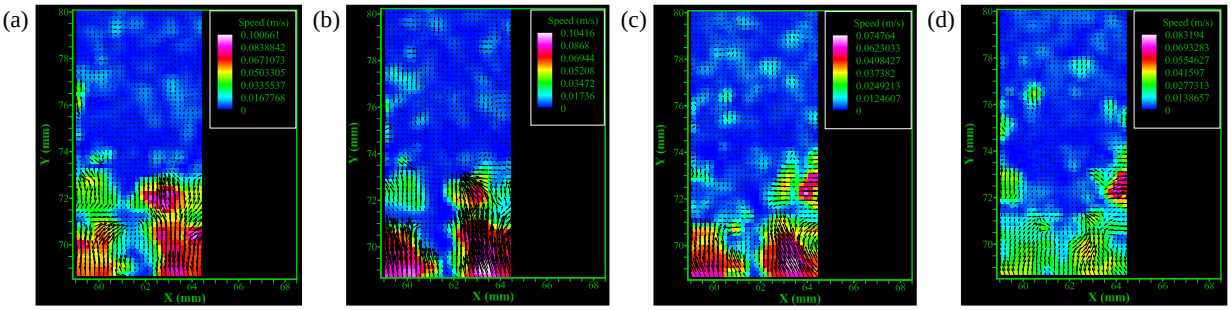

Fig. 3. Velocity fields of imbibition in circular tube with r = 0.00025 m at different time. (a) t = 0 s, (b) t = 0.1667 s, (c) t = 0.3333 s, (d) t = 0.5 s.

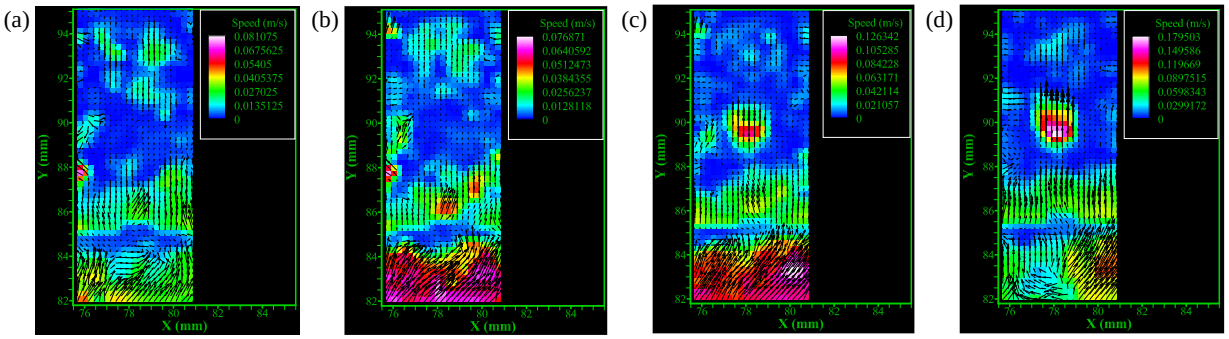

Fig. 4. Velocity fields of imbibition in circular tube with r = 0.0005 m at different time. (a) t = 0 s, (b) t = 0.1667 s, (c) t = 0.3333 s, (d) t = 0.5 s.

where $1 \leq j \leq i$, j^{th} represents the inclination angle of the j^{th} tube section, i denotes the order of tube section where the water-gas interface is located, k denotes the counting variable, and h_k is the length of the k^{th} tube section.

The above expression is the differential equation of h with respect to t, which can be solved numerically by the Euler method. The water level rising in the capillary leads to the decrease in the water level in the glass tank and further affects the actual increase in imbibition length. The water uptake model in fractures (Wang et al., 2021) is adopted. The correction coefficient relates to the capillary cross-sectional area of the water source area exposed to the atmosphere. The net length and width of the glass tank in this experiment are 0.4 m and 0.2 m, respectively. Thus, the water source area exposed to the atmosphere is 0.08 m^2. The values of the remaining parameters are the dynamic viscosity coefficient of water at 1.010×10^{-3} Pa·s, the density of water at 0.998×10^{3} kg/m^3, the phase permeability in the tube at $r^2/8$, the surface tension of water-air interface at 25×10^{-3} N/m, and the gravitational acceleration at 9.8 m/s^2. The inclination angle and wetting angle can be obtained from the experimental photographs. The initial velocity of water can be measured by PIV. A series of data on the length and velocity of water injection in the capillary can be obtained by numerical simulation.

4. Modification of the model

In the experiment, the velocity fields of water in two straight circular tubes with r = 0.25 mm and r = 0.5 mm at different times are obtained through PIV measurement, as shown in Figs. 3 and 4. The time interval between adjacent velocity fields is 1/6 s. The capillary phenomenon is not obvious and the velocity field is difficult to be obtained accurately in a circular tube with variable inclination angle. It is found that there is almost no difference between the results of displacement and velocity by numerical simulation based on different initial velocities. Therefore, regarding the value of initial velocity as zero has no significant effect on the results.

The images collected in the imbibition process are shown in Figs. 5-7. The time interval between adjacent images is 1/6 s, and the water in the capillary appears grey or bright white.

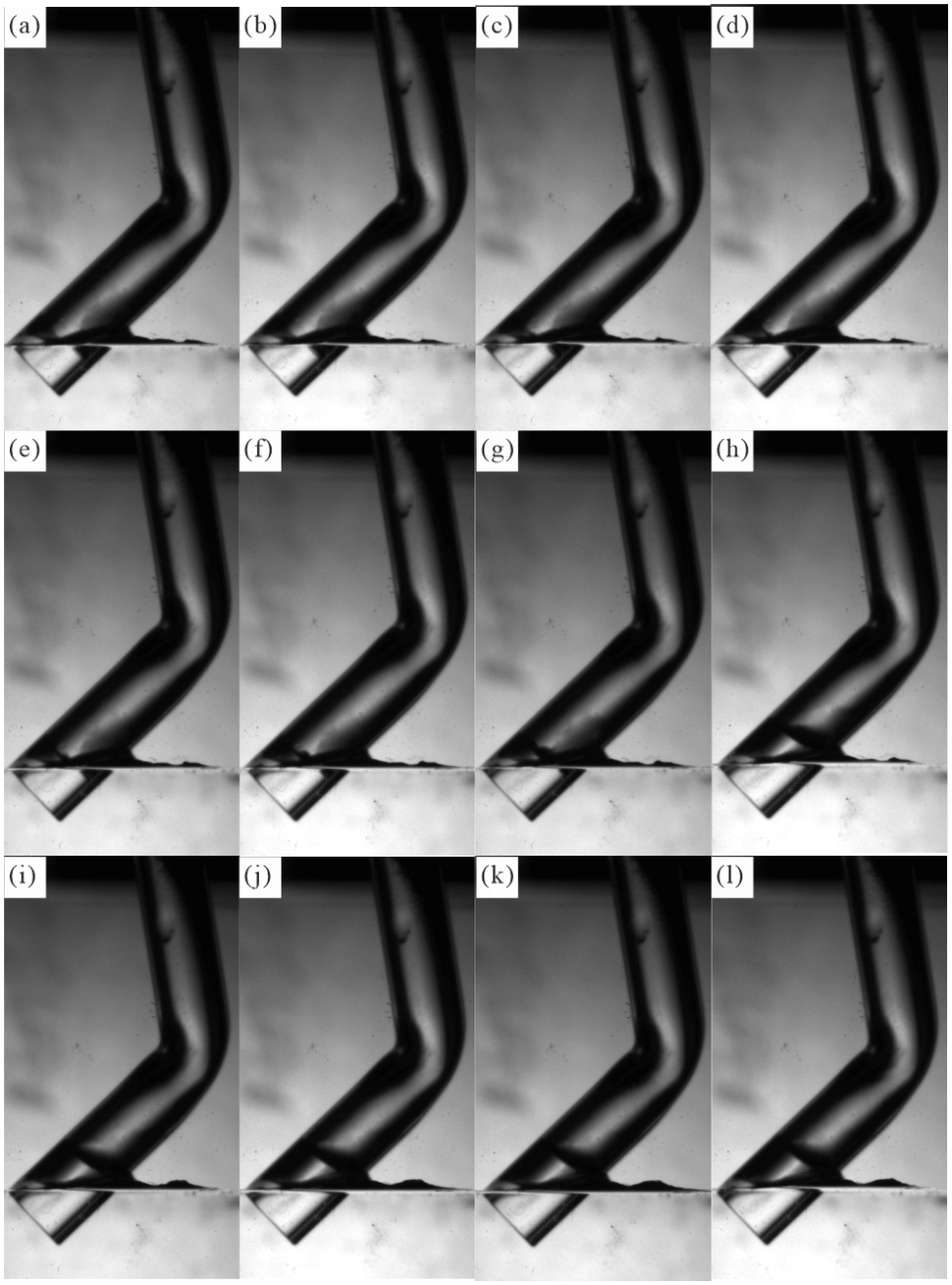

Fig. 5. Images of imbibition in circular tube with variable inclination angle at different time. (a) t = 0 s, (b) t = 0.1667 s, (c) t = 0.3333 s, (d) t = 0.5 s, (e) t = 0.6667 s, (f) t = 0.8333 s, (g) t = 1 s, (h) t = 1.1667 s, (i) t = 1.3333 s, (j) t = 1.5 s, (k) t = 1.6667 s, (l) t = 1.8333 s.

Table 2. Relationship between Tolman length and inner radius.

Inner radius (mm)	2.5	0.25	0.5
Tolman length (mm)	11.0	-1.0	-4.3

From the images, the length of water injection in the capillary as a function of time can be obtained.

In the numerical simulation, different values of Tolman length are used to fit the experimental results; the values are varied until the numerical simulation results are generally consistent with the experimental results and the error is small, and then the relevant value can be regarded as Tolman length. After several numerical simulations, the values of Tolman length of water imbibition in the three kinds of capillary tubes are determined as 0.0110 m, −0.0010 m and −0.0043 m, respectively. The relationship between Tolman length and inner radius is summarized in Table 2. It can be seen that the Tolman length decreases first and then rises with the increase in the radius of curvature of liquid-gas interface, which changes from negative to positive. The numerical results and experimental results are plotted in the same coordinate

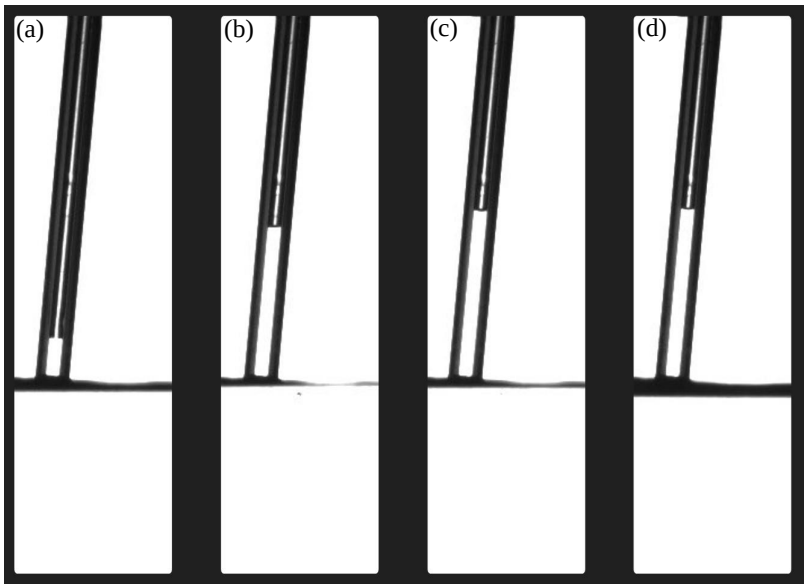

Fig. 6. Images of imbibition in circular tube with r = 0.00025 m at different time. (a) t = 0 s, (b) t = 0.1667 s, (c) t = 0.3333 s, (d) t = 0.5 s.

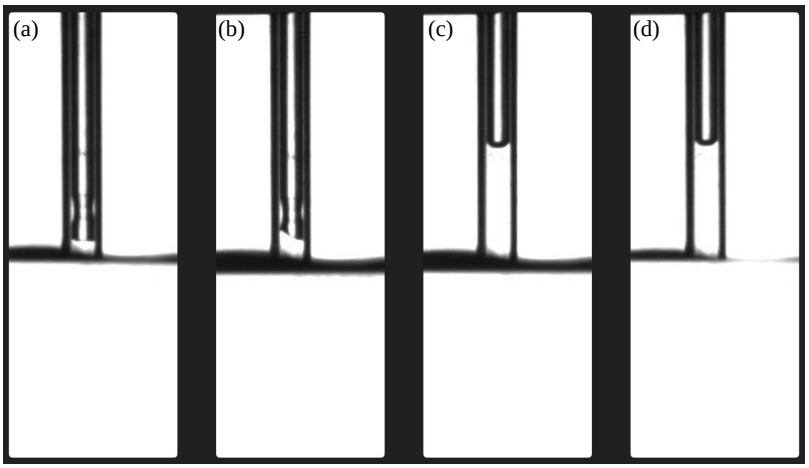

Fig. 7. Images of imbibition in circular tube with r = 0.0005 m at different time. (a) t = 0 s, (b) t = 0.1667 s, (c) t = 0.3333 s, (d) t = 0.5 s.

system, as shown in Figs. 8-10. It can be observed that the Tolman length-based LW imbibition model can better describe the imbibition processes under real conditions.

In the experiment, it is observed that imbibition does not take place immediately as water contacts the capillary tube bottom, and there is a shielding effect. Therefore, it is meaningful to study the law of wetting liquid movement in the capillary tube at the beginning of the imbibition stage. In addition, an anomaly can be observed in a tube with a constant radius: the water level rises to a small height and then stagnates. Then, it continues to rise to the maximum height and then stops again. The possible reason is that the physical properties of the inner wall of the capillary, such as dynamic contact angle, are not uniform or continuous, which leads to a phenomenon that is different from the ideal model. In this work, the initial moment is defined as the moment when the water level stops at a small height and imbibition has just begun, and the relevant data are drawn into the coordinate system. A surface wave will be generated when the water level rises in the glass tank and contacts the capillary tube, resulting in the non-zero initial velocity or initial height of the water involved in imbibition. The specific value needs to be obtained more accurately and is used in the numerical simulation algorithm as the initial condition. It can be seen that is beneficial to improve the accuracy of experimental observation and reduce the shadow caused by the capillary rise of water source on the inner wall of glass tank.

According to the actual shape and position of the water column, the corresponding position in the velocity field diagram can be obtained to draw the overall movement velocity

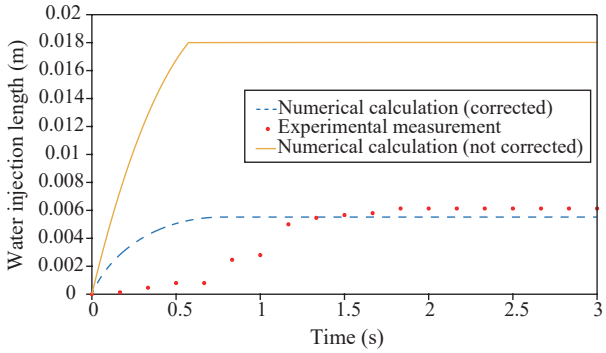

Fig. 8. Length-time data from the experiment and numerical simulation of imbibition in a circular tube with variable inclination angle.

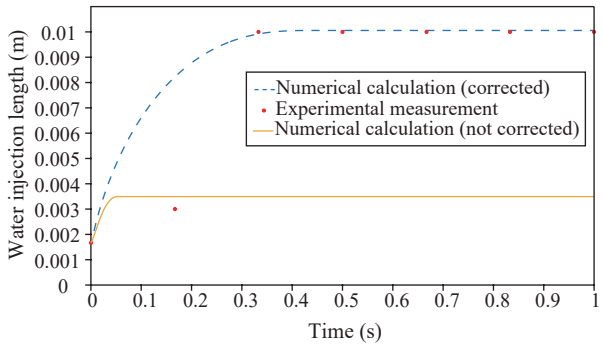

Fig. 10. Length-time data from the experiment and numerical simulation of imbibition in a circular tube with r = 0.0005 m.

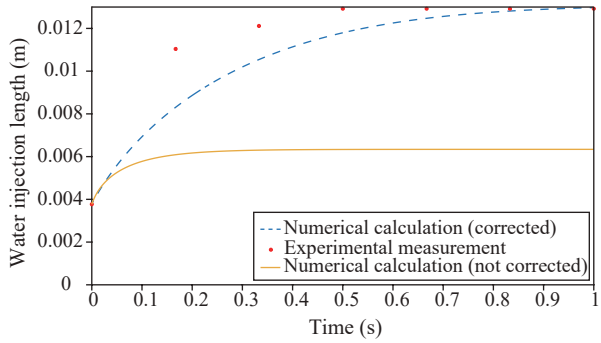

Fig. 9. Length-time data from the experiment and numerical simulation of imbibition in a circular tube with r = 0.00025 m.

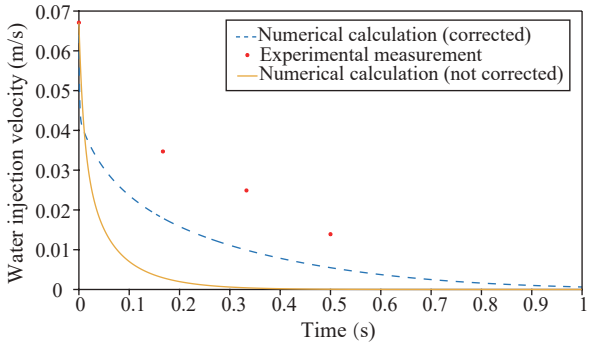

Fig. 11. Velocity-time data from the experiment and numerical simulation of imbibition in a circular tube with r = 0.00025 m.

of the fluid. The velocity-time relationships of water in the modified and classical LW imbibition model are calculated by numerical simulation, and they are plotted in the same coordinate system. The velocity-time image of the tube with r = 0.00025 m is shown in Fig. 11.

It can be observed from Fig. 11 that the LW imbibition model modified by Tolman length can more accurately describe the velocity-time relationship. As already observed from Figs. 3 and 4, the flow rules of different parts of the water column are considerably different. Therefore, different methods to measure the overall velocity may lead to different measurement errors. In addition, due to the refraction of the circular tube to the laser, the velocity field diagram presents some deviations. The uneven distribution of tracer particles also impacts the accuracy of the velocity field diagram. The measurement accuracy of the overall velocity of fluid can be improved by selecting parameters that can better reflect the overall law of fluid motion, reduce the refraction of glass tube as well as make the distribution of tracer particles more even in water.

5. Conclusions

In this work, the Tolman length in a specific circular tube is measured through laboratory experiments. The LW imbibition model is further improved by substituting Tolman length as a parameter, so as to describe the imbibition processes more accurately. The fluid-wall friction is also involved in the resistance term of the modified LW imbibition model. The main conclusions of this study are as follows:

1) Tolman length can be used as an effective parameter of the modified LW imbibition model to improve the model accuracy. The values of Tolman length under different conditions can be approximately determined by the imbibition experiments.
2) The experimental results show that Tolman length decreases first and then increases with the radius of curvature of liquid-gas interface.
3) Compared to the classical model, the Tolman length-based model performs better in describing the real imbibition process.

Conflict of interest

The authors declare no competing interest.

References

Aslannejad, H., Loginov, S. V., van der Hoek, B., et al. Liquid droplet imbibition into a thin coating layer: Direct pore-scale modeling and experimental observations. Progress in Organic Coatings, 2021, 151: 106054.

Bhatt, P. A., Mishra, S., Jha, P. K., et al. Size-dependent surface energy and Tolman length of TiO_2 and SnO_2 nanoparticles. Physica B: Condensed Matter, 2015, 461: 101-105.

Brabazon, J. W., Perfect, E., Gates, C. H., et al. Spontaneous imbibition of a wetting fluid into a fracture with opposing fractal surfaces: Theory and experimental validation. Fractals, 2019, 27(1): 1940001.

Cai, J., Chen, Y., Liu, Y., et al. Capillary imbibition and flow of wetting liquid in irregular capillaries: A 100-year review. Advances in Colloid and Interface Science, 2022, 304: 102654.

Cai, J., Jin, T., Kou, J., et al. Lucas-Washburn equation-based modeling of capillary-driven flow in porous systems. Langmuir, 2021, 37(5): 1623-1636.

Cai, J., Yu, B., Mei, M., et al. Capillary rise in a single tortuous capillary. Chinese Physics Letters, 2010, 27(5): 054701.

Cito, S., Ahn, Y. C., Pallares, J., et al. Visualization and measurement of capillary-driven blood flow using spectral domain optical coherence tomography. Microfluidics and Nanofluidics, 2012, 13(2): 227-237.

Hanžič, L., Kosec, L., Anžel, I. Capillary absorption in concrete and the Lucas-Washburn equation. Cement and Concrete Composites, 2010, 32(1): 84-91.

Karimaie, H., Torsæter, O. Effect of injection rate, initial water saturation and gravity on water injection in slightly water-wet fractured porous media. Journal of Petroleum Science and Engineering, 2007, 58(1-2): 293-308.

Kim, E., Whitesides, G. M. Imbibition and flow of wetting liquids in noncircular capillaries. The Journal of Physical Chemistry B, 1997, 101(6): 855-863.

Kou, J., Sun, S. Multi-scale diffuse interface modeling of multi-component two-phase flow with partial miscibility. Journal of Computational Physics, 2016, 318: 349-372.

Lucas, R. Ueber das Zeitgesetz des kapillaren Aufstiegs von Flüssigkeiten. Kolloid-Zeitschrift, 1918, 23(1): 15-22.

Markl, D., Wang, P., Ridgway, C., et al. Resolving the rapid water absorption of porous functionalised calcium carbonate powder compacts by terahertz pulsed imaging. Chemical Engineering Research and Design, 2018, 132: 1082-1090.

Mason, G., Morrow, N. R. Capillary behavior of a perfectly wetting liquid in irregular triangular tubes. Journal of Colloid and Interface Science, 1991, 141(1): 262-274.

Mayer, R. P., Stowe, R. A. Mercury porosimetry-breakthrough pressure for penetration between packed spheres. Journal of Colloid Science, 1965, 20(8): 893-911.

Meng, Q., Zhao, L., Li, P., et al. Experiments and phase-field simulation of counter-current imbibition in porous media with different pore structure. Journal of Hydrology, 2022, 608: 127670.

Rekhviashvili, S. S. Size dependence of the surface tension of a small droplet under the assumption of a constant Tolman length: Critical analysis. Colloid Journal, 2020, 82(3): 342-345.

Salama, A. On the dynamics of a meniscus inside capillaries during imbibition and drainage processes: A generalized model, effect of inertia, and a numerical algorithm. Physics of Fluids, 2021, 33: 082104.

Schoelkopf, J., Gane, P. A. C., Ridgway, C. J., et al. Practical observation of deviation from Lucas-Washburn scaling in porous media. Colloids and Surfaces A: Physicochemical and Engineering Aspects, 2002, 206(1-3): 445-454.

Tian, W., Lu, S., Zhang, J., et al. NMR characterization of fluid mobility in low-permeability conglomerates: An experimental investigation of spontaneous imbibition and flooding. Journal of Petroleum Science and Engineering, 2022, 214: 110483.

Tolman, R. C. The effect of droplet size on surface tension. The Journal of Chemical Physics, 1949, 17(3): 333-337.

Wang, J., Kou, J., Cai, J., et al. Tolman length-based modified Lucas-Washburn capillary-driven model and numerical simulation. Chinese Journal of Computational Physics, 2021, 38(5): 521-533. (in Chinese)

Wang, J., Liu, H., Qian, G., et al. Investigations on spontaneous imbibition and the influencing factors in tight oil reservoirs. Fuel, 2019, 236: 755-768.

Wang, X., Wang, M., Li, Y., et al. Shale pore connectivity and influencing factors based on spontaneous imbibition combined with a nuclear magnetic resonance experiment. Marine and Petroleum Geology, 2021, 132: 105239.

Wang, J., Zhu, X., Pan, Y., et al. Water uptake in parallel fractures. Capillarity, 2021, 4(1): 1-12.

Washburn, E. W. The dynamics of capillary flow. Physical Review, 1921, 17(3): 273-283.

Zahasky, C., Benson, S. M. Spatial and temporal quantification of spontaneous imbibition. Geophysical Research Letters, 2019, 46(21): 11972-11982.